

# Dynamics and Control of Microwave Granular Imager

Marco B. Quadrelli, Darmindra Arumugam  
Jet Propulsion Laboratory, California Institute of Technology  
4800 Oak Grove Dr.  
Pasadena, CA 91109  
818-354-7548  
marco.b.quadrelli@jpl.nasa.gov

**Abstract**— Granular media in space can be used in the radar and microwave bands to enable imaging of previously inaccessible regions of targets with high geophysical variations with time, such as comets. The means of imaging, which includes a re-direction of energy, can permit higher resolution imaging as well. Applications include both tomographic and topographic radar imaging. The effect of the granular media cloud geometry plays a significant role in the scattering process. In addition, the spatial randomness effects the beam collimation and can have a positive effect on the imaging qualities in terms of effective aperture, coverage, and resolution of the radar techniques.

## TABLE OF CONTENTS

1. INTRODUCTION .....	1
2. THE ORBITING RAINBOWS PARADIGM .....	2
3. APPLICABILITY OF GRANULAR IMAGER TO EARTH AND PLANETARY SCIENCE .....	3
4. RADAR SYSTEM ARCHITECTURES .....	5
5. RADAR MODELING AND SIMULATION .....	6
6. RADAR EXPERIMENTS .....	16
7. CONCLUSIONS .....	17
ACKNOWLEDGEMENTS .....	18
REFERENCES .....	18
BIOGRAPHY .....	19

## 1. INTRODUCTION

“Orbiting Rainbows” ([1, 2, 3, 4, 5, 6]) is a NASA Innovative Advanced Concepts (NIAC) study that is looking twenty years into the future of creating a space-based observatory from granular media. The goal of this research was to identify ways to optically manipulate and maintain the shape of a cloud of dust-like matter so that it can function as an adaptive surface with useful electromagnetic characteristics in the optical or microwave bands. The investigators are performing fundamental research and developing the technology roadmap to construct an imaging system in space using nonlinear optical properties of a cloud of micron-sized particles, shaped into a specific surface by light pressure, to form a very large and lightweight aperture of an imaging system. This “cloud optic” will be relatively simple to package, transport, and deploy. It is reconfigurable and can be re-targeted; the focal length is variable and it will be self-healing and ultimately disposable. Within the Orbiting Rainbows Project, we have been developing radar

instrument architectures that use cloud physics and scattering to enable tomographic imaging in previously inaccessible areas of bodies (comets, asteroids) - Rayleigh or small particle approximations is used to model cloud physics.

The problem of using granular media to aid in microwave imaging requires the study of two general bodies of problems. The first general problem involves the vector radiative transfer theory to describe the exact phase sensitive scattering of incident waves by the granular medium, which may be complex in nature with various particle sizes, distributions, and dielectric and conductive properties. We developed two types of forward simulation methods, one using analytical series expansion of the scattered field – for a quick simulation of scattering from finite spheres, and the second using finite-difference time-domain (FDTD) to simulate full-wave scattering of arbitrarily shaped objects. We used the simulations to develop a reconstruction algorithm using time-domain back-projection, and verified that it worked correctly using the simulated results from simple scatterers. In addition, we conducted experiments to first verify the time-domain back-projection algorithm. The next step, was to develop a radiative transfer model that permits multiple scattering from the granular media, in order to re-direct the energy from/to the target. We developed this using exact TE and TM derivation using electromagnetic potentials and boundary conditions on spheres. Once the transfer model was complete, we studied the re-directing of signaling using some simplified structures for granular media. Specifically, we studied the planar mirror as a prototype problem. Experiments were also conducted to verify the validity of the models and algorithms. In these experiments, we used a planar reflector to re-direct the energy and image a target through the re-directed energy, scattered through the planar reflector. The second general problem involves the exact image inversion theory based on phase sensitive scattering of a general distributed scene to be imaged – which may also contain various inclusion/target sizes, distributions, and dielectric and conductive properties. For this second topic, we developed imaging techniques to enable imaging of the granular media for feedback control. We used a cloud physics simulator to derive a shrinking and rotating cloud, and used imaging algorithms to invert and image the granular media cloud in 2D space.

Section 2 describes the Orbiting Rainbows paradigm. Section 3 discusses the radar system architectures under consideration. The approach for radar system modeling and simulation is discussed in Sections 4 to 10. Section 11 summarizes the results of the radar experiments.

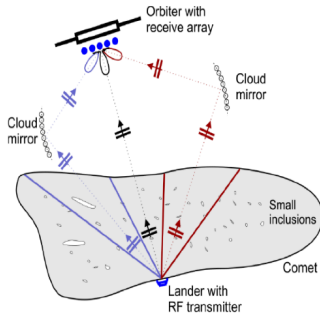


Figure 1. Tomographic imaging with Granular Imager.

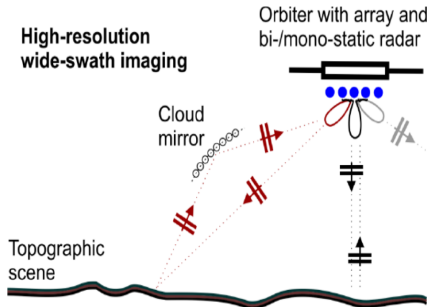


Figure 2. Topographic imaging with Granular Imager.

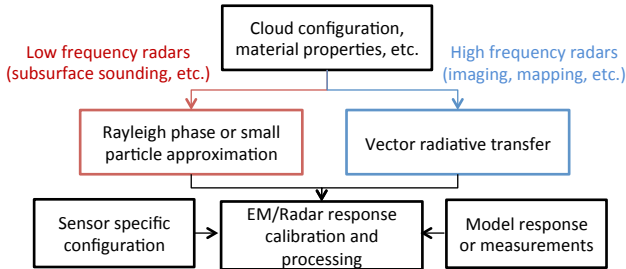


Figure 3. Elements of radar system architectures.

## 2. THE ORBITING RAINBOWS PARADIGM

Recent work [1, 2, 3, 4, 5, 6] has investigated the feasibility of a granular imaging system, concluding that such a system could be built and controlled in orbit, and could be used effectively as an imaging system in the radar and visible bands. Finding a way to manipulate such distribution of matter in space would lead to a potentially affordable new way of generating very large imagers in space, and open the way to revolutionizing large-scale antennas. Our concept is to enable the large-scale electromagnetic utilization of an active cloud of incoherent matter. With near-term plans to build 30 meter ground-based telescopes for astronomy and similar apertures for remote sensing, the demand for higher resolution optics in space continues to grow not only for exoplanet detection, but also for earth-based science, including hyper-spectral imaging and for monitoring of the oceans and land masses (e.g. seismic monitoring). Compared to conventional large aperture systems, our proposed concept is

unique in that: a) it would be a structure-less, very lightweight system, leading to areal densities of 0.01 kg/m<sup>2</sup> or less, compared to 10 kg/m<sup>2</sup> or more of monolithic apertures; b) one cloud could combine with other clouds to form extremely large apertures; c) would be easy to package, not requiring structural elements; d) line-of-sight retargeting and figure control would be realized remotely using electromagnetic fields, without the need for complex sensors and actuators on the backing structure. These properties enable new mission architectures, and are in contrast to current state-of-the-art systems which are limited to much smaller sizes and are quite massive. The paradigm that makes this granular imager possible is based on: a) avoiding any physical structure and sensing/actuation hardware on the primary aperture; b) using at-a-distance trapping and manipulation to confine and shape the cloud acting as primary; and c) relaxing the optical figure control requirements via state-of-the-art computational imaging algorithms. In our initial effort, focused on the astrophysical and radar tomography applications of the Granular Imager, we have: a) gained initial insight into the physics of granular systems in space; b) developed an approach to trap and align a cloud of reflective particles; c) designed reflective, refractive, and diffractive imaging systems that include multistage wavefront control to compensate for uncorrectable errors due to the stochastic nature of the cloud; d) identified multi-frame blind deconvolution algorithms that reconstruct image estimates from an ensemble of incoherent images; e) developed empirical electromagnetic models to study the granular medium reflective and transmissive response in the microwave band; and f) developed a preliminary multi-scale simulation, which predicts the time evolution of the imaging system kept in formation as it orbits the Earth. A typical orbital scenario would follow these steps: (1) the cloud is first released; (2) it is electromagnetically trapped to avoid dissipation and disruption by gravitational forces and shaped into a two-dimensional object (coarse figure control); and (3) the grains could be aligned to the incoming wavefront by means of rastering laser beams (fine figure control) leading to a surface with acceptable imaging characteristics, i.e. the primary aperture. By modulating the spatial and temporal distribution of the confining fields, the cloud can be retargeted as desired. The secondary would be in formation flight with the primary aperture. Established computational imaging techniques would process the sequence of images to remove additional noise (scattering, speckle) and further improve the image quality. Beam shaping of a cloud of particles is possible by molding the cloud with the gradient force, say in the x-y plane, and by further molding the cloud in the z-direction by the combined optical scattering force and gravitational forces arising from the orbital dynamics (tidal forces). For a grain radius of 1 micron, the irradiance in the vacuum of space at a temperature of 10 K required to “freeze” the distribution can be estimated to be of the order of 13 kW/m<sup>2</sup>, a CW laser power level which is within the range of commercial lasers in the visible band, including Nd:YAG laser at 532 nm.

### 3. APPLICABILITY OF GRANULAR IMAGER TO EARTH AND PLANETARY SCIENCE

Large light-weight aperture collectors and high-efficiency detectors are identified as a critical technology both in microwave and optical technology applications within and without NASA [19, 20, 21]. In general, deployable large apertures can relax requirements on transmitter technologies (because of the higher gain provided), enable measurement scenarios from small satellite platforms, and enable observations with sufficient resolution from specific vantage points such as Sun-Earth Lagrangian Points (L1, L2) or Geostationary orbit. In [17], the possibility of imaging the propagation of seismic waves from a very large space-based optical telescope is discussed. Images of seismic waves propagating at the Earth's surface would be an invaluable source of information for investigating earthquake physics and the effect of the subsurface on earthquake ground motions. This application would require ground displacement measurements at about every 100 m, with cm accuracy, and temporal sampling on the order of 1 Hz. A geostationary optical telescope with a large aperture appears to be the most promising system, and [18] considers a telescope with an angular field of view of  $0.8^\circ$  and with an aperture greater than 4 m, and show that key details of the seismic wave field, hardly detectable using ground-based instruments, would indeed be imaged by such a system. Another application is in the area of atmospheric spectroscopy from L2, as discussed in [16,17]. There are strong scientific motivations for placing an Earth observatory at L2. The occultation due to the orbital geometry at L2 is best suited for long-term climate change studies. We can obtain high vertical and spatial resolution maps of many chemical species twice per day for the use in near-real time predictive assimilation models. A similar capability would require a constellation of multiple spacecraft in low Earth orbit. Near real-time production of the final products for time-critical consumption (forecast models) would be feasible. The co-alignment of the spectrographic instruments and the synchronization of the operations of a large aperture system in formation with a detector spacecraft would provide a sampling of the same air mass over a wide band of wavelengths (0.25 to 10.5 microns). Atmospheric monitoring would involve obtaining global maps of the vertical distribution of O<sub>3</sub>, CO<sub>2</sub>, CH<sub>4</sub>, H<sub>2</sub>O, N<sub>2</sub>O, key members of the NO<sub>x</sub> and CL<sub>x</sub>, and the upper tropospheric and stratospheric clouds, sulfate aerosol mass, temperature, and pressure with sampling near the stratopause, twice per day. Long-lived chemical species would be used to monitor the global circulation (mean meridional and planetary wave dynamics) at a lower vertical resolution, and the changes would be observed in the tropopause region, and the stratospheric-tropospheric exchange processes. These capabilities will enable such a system to determine the changes in the forcing and the responses of the Earth's atmosphere, where forcing is due to natural and artificial factors that influences the atmosphere; to understand and quantify the mechanisms of these changes, be it of chemical or dynamical origin; to improve the short and long term

predictive capability of the climatic changes through the use of near real time measurements and an improved understanding of the dynamical, chemical, and radiative processes in the atmosphere. The required resolution for the observations of the atmosphere at the distance of L2 dictates that the telescope would need a primary mirror with an unprecedented diameter of many 10's of meters. A traditional mirror of that size, or a multi-mirror array, would have an impractical mass, and would be extremely difficult to build, and maintain with the necessary optical precision. This is where the Granular Imager becomes competitive.

For a sparse array (i.e., not a monolithic array), focusing of the beam is achieved by modulating the phase of the distributed radiators so as to obtain a conic phase surface. Previously it was observed that by randomizing the emitter positions the beam achieves better quality [30,31,32], even with highly thinned sparse arrays.

For lidar, deployable apertures larger than 2 m would enable reduced laser power or improve system performance, and could enable some missions from smallsats [11]. Athermal large aperture field-widened interferometers are needed for wind and aerosols. An emerging technology is miniaturization: the burgeoning additive manufacturing field offers potential solutions for previously impossible enabling constructs (e.g., large-area mirrors that are light-weighted in ways that cannot be accomplished through other means). An emerging ancillary receiver technology is large effective area, lightweight telescopes, with areal density  $< 25 \text{ kg/m}^2$ , and  $> 3 \text{ m}$  aperture diameter.

For microwave applications apertures of several tens of m would enable observations of earth from Geostationary Orbit at spatial and temporal resolution sufficient to resolve the evolution of several processes related to weather and the water cycle [22]. Among the several microwave applications requiring GEO deployment of large apertures summarized in [22] we note: water vapor, hurricanes, biomass, winds. In general, the great advantage of GEO or Lagrangian Point observations (that is, providing a time-continuous record capable to resolve various processes as they evolve) is countered by the significant investments necessary to develop very large instruments necessary to achieve sufficient horizontal resolution. LEO solutions are often simply the workable compromise where affordability becomes the fundamental limiting factor. For active systems (i.e., radars) the problem of GEO and Lagrangian Point is further exacerbated by the transmit power needed to obtain detectable returns. Once again, the use of very large apertures is, in principle, capable of mitigating this aspect because of the higher gain provided by the aperture.

Rather than attempting to enumerate in how many scenarios an extremely large and tenuous aperture could enable Earth Science measurements that cannot otherwise be achieved, we will provide here a few representative examples. A 35 GHz radar, with a 35 m primary reflector, was identified more than a decade ago as a viable solution to place a Hurricane monitoring radar in GEO [26, 14]. Several key technologies were developed and demonstrated, and the final hurdle was confined to the actual engineering and

financial challenges associated with the implementation of a full scale instrument to be deployed. The measurement concept remains desired by the scientific and operational hurricane communities and yet despite the specific encouragement in [22], little progress has been made in the last decade to make this instrument any more affordable. Furthermore, its size was already a compromise, since, ideally, an aperture of a 200 m would have been truly the definitive answer (to provide an horizontal resolution of 2 instead of 12 km). That concept relied on a spherical reflector geometry, with a feed array designed with fixed configuration to pre-compensate for the resulting constant aberration and moving mechanically to achieve angular scan and the desired coverage of the central Atlantic, low sidelobe pulse compression and a 150W solid state power amplifier completed the configuration to achieve the desired detection of light precipitation (i.e., 10 dBZ). Fast forward to present time. Digital and electronic scanning active phased array technologies have advanced as expected demonstrating that the feasibility and affordability of the feed.

If GI technology were to mature in the next few years, and a 200 m hemispherical shell were to become feasible, it would suffice to radiate a few tens of Watts (similar to for example the RainCube from a 6U cubesat [23]) to achieve continuous monitoring of hurricanes at a 2 km horizontal resolution. Going to longer wavelengths, an aperture of this class could enable for example biomass and soil moisture monitoring across the diurnal cycle at horizontal resolutions of 10-30 km. Going to shorter wavelengths one could envision instruments in the IR deployed at Sun-Earth L1 to provide time continuous radiation budget measurements that account in real time for the incoming solar radiation. The principle of GI could also potentially augment closer-to-Earth systems in LEO by enabling larger apertures because of higher deployed-to-packed size ratios.

To accomplish the goals for Earth science, spatial coherence at low frequency, or the aperture rigidity in orbit, must be achieved, by relative grain control. The system libration dynamics in orbit must be stable, i.e. the attitude dynamics of the aperture must be stable with respect to the local orbiting frame. This can be achieved by a favorable orbital distribution of the grains. [8,9] consider large swarm arrays of picosats for Astrophysics and Earth science. In addition, large swaths of the Earth could be continuously monitored with an extremely fault-tolerant system. Also, spatial coherence at high frequency must be achieved, and could be obtained by containing the cloud dispersion electromagnetically. Finally, the signal transmitted or received by the aperture must exhibit spatio-temporal phase coherence so that intensity at the maximum peak lobe of the array pattern is maintained. This could be achieved by limiting the differential effects of orbital perturbations. The incoming signal must be also in phase to within the diffraction limit to add coherently (this amounts to approx. 1 cm of relative grain motion within the cloud at 1.4 GHz). The motion of elements near the symmetry axis will cause defocus, and higher order aberrations (coma, astigmatism) result from motion of the off-axis elements from the figure

plane. Consequently some form of figure control (i.e. wavefront control) is necessary. Also, to accommodate multiple look angles (i.e., boresight control), the plane of the aperture must be able to tip/tilt as an equivalent rigid aperture. The determination of the effective aperture size and cloud density to fill the aperture, will depend strongly on the chosen wavelength, the noise-equivalent temperature at the detector, and also on the diffraction limited ground resolution, surface reflectivity, dwell time, ground spot diameter, and source temperature.

In this regard, Figure 22 shows the ground resolution vs. fill factor of GI passive radiometer at GEO at several wavelengths, showing that the resolution would increase, as expected, with GI fill-factor (nominally, we used 10,000 grains in the calculation). Preliminary trends of the GI performance as a passive or active radiometer from GEO looking at a spot on the ground at 1.4 GHz, for three different grain sizes, are shown in Figures 23, 24, and 25, indicating that adequate performance, quantified as detector area and achievable ground resolution, can be achieved with a much lower mass GI, and that the total number of grains would much smaller in the case of an active system.

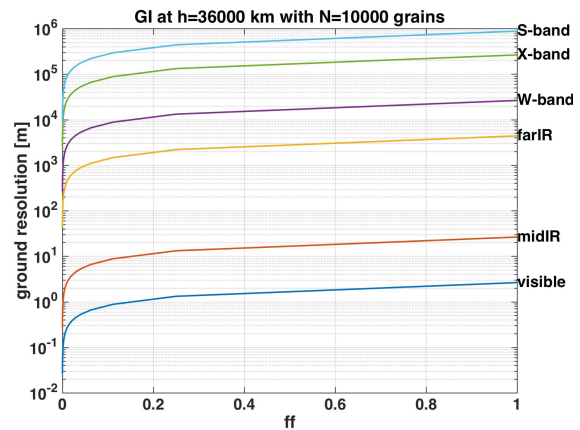


Figure 4. Ground resolution vs. fill factor of GI passive radiometer at GEO.

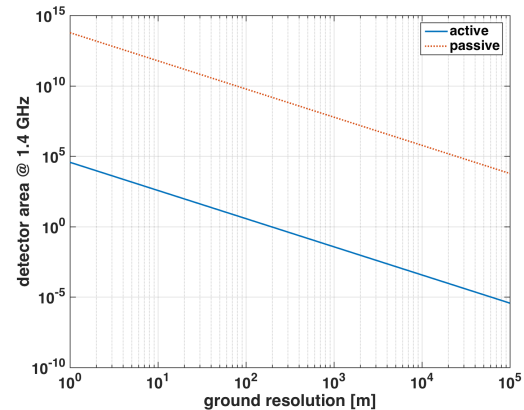
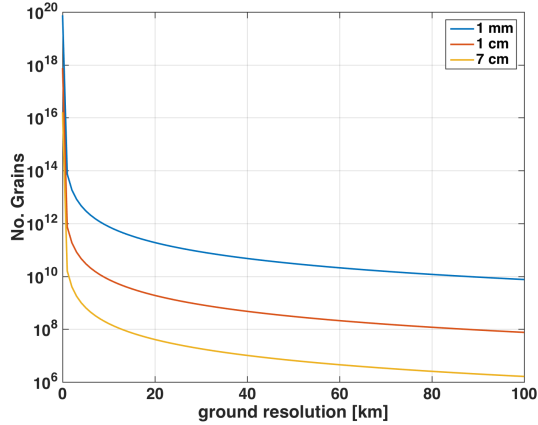
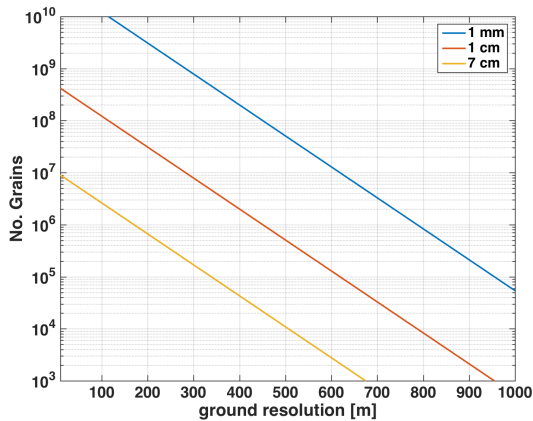


Figure 5. Detector area of passive radiometer at GEO at 1.4 GHz vs. ground resolution.



**Figure 6. Number of grains vs. ground resolution for different grain sizes for passive radiometer at GEO at 1.4 GHz.**



**Figure 7. Number of grains vs. ground resolution for different grain sizes for active 100kW radiometer at GEO at 1.4 GHz.**

#### 4. RADAR SYSTEM ARCHITECTURES

The objective of the radar modeling and simulations work was to investigate the conditions to manipulate and maintain the shape of an orbiting cloud of dust-like matter so that it can function as an ultra-lightweight surface with useful and adaptable electromagnetic characteristics in the RF, or microwave bands. The proposed cloud architecture is to construct an optical system in space in which the nonlinear optical properties of a cloud of micron-sized particles are shaped into a specific surface by light pressure, allowing it to form a very large and lightweight aperture of an optical system, hence reducing overall mass and cost. Other potential advantages offered by the cloud properties as optical system involve possible combination of properties (combined transmit/receive), variable focal length, combined refractive

and reflective lens designs, and hyper-spectral imaging.

A cloud of highly reflective particles of micron size acting coherently in a specific electromagnetic band, just like an aerosol in suspension in the atmosphere, would reflect the Sun's light much like a rainbow. The only difference with an atmospheric or industrial aerosol is the absence of the supporting fluid medium. This new concept is based on recent understanding of the physics of optical manipulation of small particles in the laboratory, and the engineering of distributed ensembles of spacecraft swarms to shape an orbiting cloud of micron-sized objects. While achieving the feasibility of constructing one single aperture out of the cloud is the main topic of this work, it is clear that multiple orbiting aerosol lenses could also combine their power to synthesize a much larger aperture in space to enable challenging goals such as exoplanet detection.

The concept and potential of these granular media extends into the microwave bands, where active imaging can be performed in the radar bands through either refocusing or redirecting energy scattered from targets and mediums. Conceptually, the goal within the radar bands, which include RF, or microwave, is to develop active radar techniques that use cloud physics and scattering through granular media in space to enable:

1. Tomographic imaging: Imaging in previously inaccessible areas of bodies (comets, asteroids, etc.) and
2. Topographic imaging: Higher-resolution imaging through focusing (ground mapping, etc.).

The purpose of this innovation is simple: when a satellite sensor mission is employing synthetic aperture imaging (SAR) imaging, the imaging resolution is high in the azimuth direction (directing of sensor motion), but low in the cross-track direction (direction perpendicular to the sensors motion). For target bodies with little geophysical activity, this is not problematic since the satellite will eventually sense the entire object and be able to integrate all the data to obtain imaging of the interior. However, for target bodies with high activity, simultaneous high-resolution cross-track imaging is extremely desirable. These include targets such as comets, which are of current interest to the science and geophysics community. While this can be achieved through use of multiple or many satellite radar sensors, there is usually a prohibitive cost associated with additional satellites or sensors.

To summarize, the granular medium can be used to image previously inaccessible regions of these target bodies, or perform higher resolution imaging, by redirecting or focusing energy scattered by these bodies in such a way that permits very large aperture SAR imaging through a very limited aperture. A direct application of this is the simultaneous high-resolution cross-track SAR imaging that can be accomplished using scattering through granular media in space. Radar remote sensing instruments that use radar imaging and sounding enable the exploration of planets, comets, asteroids, their atmospheres and interiors at higher resolutions than possible with other non-penetrating

instrumentation. Due to continued success in scientific exploration of these subjects, the next generation of remote sensing architectures will demand even higher resolutions to enable more detailed probing and experimentation. Generally speaking, radar resolution has two components: the “range” resolution and the “azimuth” resolution. These are determined by many factors, including the wavelength of the electromagnetic excitation and the intervening medium within which the electromagnetic wave propagates. Traditionally, radar instrument resolutions have frequently been limited by the characteristic of the medium due to propagation losses, dispersion, and coherence property of the medium. For example, low-frequency sounding radars such as the Mars Advanced Radar for Subsurface and Ionosphere Sounding (MARSIS) is able to detect what lies beneath the surface of Mars (up to about 3 km), but at a low azimuth resolution due to ionospheric scattering and dispersion. MARSIS operates with a very high fractional bandwidth: 1 MHz bandwidth allows a vertical resolution of 150 m in vacuum, which corresponds to 50–100 m in the subsurface. MARSIS is an unfocused synthetic aperture radar with best-case along-track resolution of 2 km. Another example in sounding radars is the Mars Shallow Subsurface Radar (SHARAD) on board the NASA Mars Reconnaissance Orbiter spacecraft. SHARAD operates with a center frequency of 20 MHz and 10 MHz bandwidth. These parameters allow vertical resolution on the order of 10–20 m. Data coming from SHARAD can be processed with focusing algorithm (chirp scaling algorithm), giving a best horizontal resolution of 300 m. Another class of examples are high-frequency altimetry mapping radars such as the Poseidon 3 altimeter radar onboard the Jason 2 satellite provides high-resolution range measurements but poor along-track resolution due to practical but large antenna beam-widths.

## 5. RADAR MODELING AND SIMULATION

Our approach is to increasing the resolution of a typical radar remote sensor was to create a medium, denoted by a cloud of objects (reflectors, etc.), within which the physics of scattering or radiative transfer provides a favorable or focused result (Figure 39). This includes focusing through generation of a large aperture or through the manipulation of the array factor of the cloud reflector objects. The ability to control the resolution of such a technique would be limited to the wavelength of the excitation and properties of the cloud, such as configuration, material properties, shape, etc., as well as the instrument design and configuration. The least understood of these topics being the cloud material properties, shape of objects within the cloud, and cloud configuration. For example, radar ionospheric, atmospheric, and subsurface sounding often use long wavelengths, which allow use of the Rayleigh phase function or the small particle approximation for calculating the effect of cloud properties and configuration on the bulk electromagnetic response. On the other hand, high-resolution radar imaging, for example, interferometric topography mapping, typically using very short wavelengths preclude use of the Rayleigh phase method

or small particle approximations, and must instead be developed using Mie scattering for spherical objects, or vector radiative transfer theory, as noted in Figure 40. Use of vector radiative transfer theory will enable the analysis of the cloud in the microwave band.

### 5.1 *Methods to simulate full-wave scattering of arbitrary clouds*

The key methods to model full-wave scattering of arbitrary clouds and their effectiveness as a granular medium to image in the radar bands are developed using numerical finite differences and using a analytical exact solution based on series expansions of harmonic solutions. The numerical finite difference technique is very useful in the time-domain, and can be used to simulate relatively complex heterogeneous clouds with large relative bandwidths, however is limited by very limited ability to study the effect of variation in cloud geometry. This limitation is primarily due to the large computation and memory resources required, as well as computation time needed to conduct a numerical simulation using finite-differences. To permit numerical simulation of large spectral bandwidths via a single simulation, the finite-difference time-domain simulations are used.

When the effect of cloud geometry, particle size, spatial distribution, et cetera is required to be studied, then an analytical method is better suited as it is computationally efficient and would require substantially lower computational resources, time, and memory. The analytical technique will however have to consider multiple scattering, though it can be practically truncated via a finite series expansion of some sort. The analytical technique is typically better suited and can be convergent if constructed in the frequency domain, as opposed to the finite-difference which is the time domain. The technique developed in this work to simulate the full-wave scattering uses a boundary value method and a T-matrix solution to simulate transverse electric or transverse magnetic scattering of plane-waves via an arbitrary distribution of particles in space. To simplify the technique and convergence, the technique is developed in two-dimensions.

### 5.2 *The finite-difference time-domain modeling and back-projection technique*

The finite-difference time-domain (FDTD) technique permits simulations of the full electromagnetic interaction and propagation in space and time. FDTD utilizes uniquely defined spatial cell structures to discretize the fields in the spatial domain. The purpose of the spatial discretization is to enable numerical calculation of the electric and magnetic field in space. A common method to discretize the cells is to use the Yee-cell model as shown in Figure 41. In the three-dimensional (3D) case, the Yee grid cell is configured in such a way that the electric (E field) field grid centroid is spaced a half spatial step from the magnetic (H field) field grid centroid. In FDTD, the electric field grids throughout the

entire simulation space are updated numerically before the magnetic field grids. Through this time stepping between the electric and magnetic field, and due to the offsets in the Yee-cell model, the electromagnetic wave can be modeled for propagation and scattering behavior until all transient phenomena or steady state processes are complete. This is done by simply by calculating the electric field and magnetic field in subsequent manner under the Yee-grid configuration. FDTD allows accurate transient and steady state simulations for scattering and propagation, which makes it ideal to study scattering from complicated bodies such as a comet – both for transient analysis, and for scattering sensing or imaging purposes.

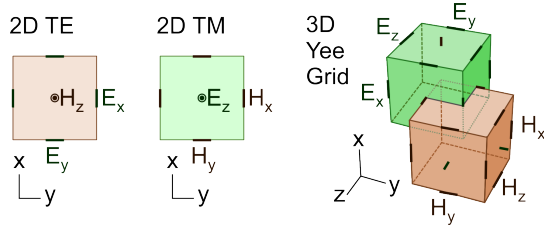


**Figure 8. The Yee grid in 3D FDTD and the limiting cases for 2D TE and TM simulations in FDTD**

FDTD can be developed for 2D or 3D. We developed FDTD for both the 2D and 3D problem.

In 2D, the simulations can take the form of the 2D transverse electric (TE) and transverse magnetic (TM) domains. In comet applications, the most common scattering stems from the transverse magnetic domain. The FDTD model used here is a 2D transverse-magnetic simulation (TM-z) [27, 25], where simulation is performed on the x-y plane cutting through the comet model. For the 2D simulations, the comet has a scale of about 4-5km on each side. The FDTD simulations were developed for an arbitrary wavelength or excitation frequency, though the simulations conducted so far focused on the 1MHz center frequency, for which the FDTD comet model can be considered electrically large. We satisfy the FDTD stability criterion using a rectangular spatial Yee-cell mesh of 1/30 of the wavelength for very good amplitude and phase stability [27]. Due to use of TM-z in the 2D simulations, the magnetic fields are parallel to the x-y plane, whereas the electric fields are perpendicular to the plane. Specifically, we use  $H_x$  to model the magnetic field along the x-direction,  $H_y$  along the y-direction, and  $E_z$  along the z-direction. The 3D FDTD simulations consider the full electromagnetic coupling (not limited to TE or TM slice), and is developed using the framework defined in Figure 41. The fields generated for the 3D FDTD is defined as an exact dipole field (by deriving the time-domain transient electric and magnetic field of a dipole in 3D space). The dipole is located at a user-defined location on the 3D space, though typically far away from actual simulations space. For comet simulations, the source dipole is typically located at 20-100km in distances from the simulation domain. The field of the dipole is complete in the sense that it accounts for the near and far fields of the comet (quasistatic, intermediate, and radiation regions). The

analytical field of the dipole in 3D space is used to calculate the electric and magnetic fields on the simulation domain. Specifically, the fields can either be injected into the simulation space at the top surface region or it can be used to calculate the fields in all regions of the 3D spatial domain. The analytical fields are calculated once before the E-H time-stepping, and the FDTD time-stepping subsequently propagates the field and waves into the simulation space transiently and until steady-state is achieved and the time-stepping is stopped.

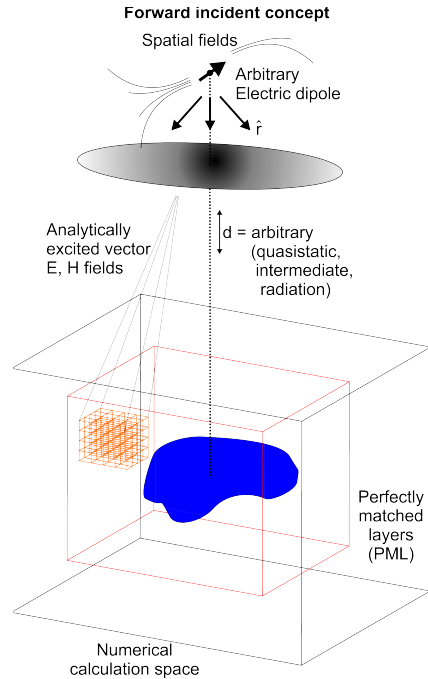


**Figure 9. Forward model for 3D FDTD to include the analytical field propagator (AFP) and the perfectly matched layers (PML)**

The comet body or the target to be simulated is located inside the simulation zone. The body needs to be discretized to the FDTD cell discretization size, and the 3D dielectric and conductivity maps for the discretized model needs to be geometrically interpolated or averaged at the sub-cell level to enable correct location and value definition of the electric material (permittivity and conductivity) and magnetic material (magnetic permeability and magnetic conductivity) properties. The electric materials must be defined on the electric Yee-grid, whereas the magnetic materials must be defined on the magnetic Yee-grid. This step is critical to ensure that the intended isotropy of the medium is preserved.

Once the FDTD time-stepping is started, the fields and waves will propagate into the simulation domain. They will then reflect off the hard outer boundary of the simulation zone, causing substantial perturbation of the sensed field (fields and waves scattered back into the simulation domain instead of propagating outward). This is due to the impedance boundary at the simulation edge, and is a major problem in full-wave numerical simulations. To solve this problem, a perfectly-matched layer (PML) is specially designed to

absorb the fields, with an effective isolation measured to about 100dB [25]. The PML (Figure 42) ensures that scattering in the computational domain is not generated when the waves hit the edge of the computational domain. One obvious value of the FDTD software developed at JPL is that it permits an arbitrary PML definition, which allows a systems engineer to control the effectiveness of the PML absorption vs. size of the FDTD domain or computing time. This is a critical feature that is not found in commercial tools and that is valuable in space research and systems engineering applications.

Once the fields and waves scatter from the target, the resultant waves will propagate outward in all directions. There will be no reflections from the edge of the simulation boundary, but the waves will not travel to the sensor either. To collect the energy of the fields and waves at the sensor, we need to calculate the scattered fields and waves at a chosen location of the sensor. We assume a mono-static sensor, for simplicity, and use the source dipole as the collector or receiver as well. We use a near-field to far-field (NFFT) transform as shown in Figure 43 to transform the field seen at the boundary of the PML to the far fields seen at the receiver dipole.

The NFFT transform uses the formalism of the surface equivalence principle. The surface equivalence principles requires calculation of the electric and magnetic vector current densities on a surface enclosing the body in order to enable calculation of the far fields. In the setup shown in Figure 43, this relates to the 8 planar surfaces at the boundary of the PML and simulation space, and on each side of the FDTD region. However, since we are interested in the mono-static scattering and since the sensor is located in the  $+z$  direction and aligned to the centroid of the top FDTD plane, it becomes only necessary to use the top plane to calculate the NFFT transform. This is indicated in Figure 43 as the colored field region. The NFFT collects these fields and converts it to the far field. This can be done in the frequency domain or in the time domain. We choose to apply the transform in the time-domain, as it permitted a manipulation that enables calculation of the far-field solution in real-time (on-the-fly).

To study the 3D FDTD simulations, we developed an integrated simulation module that permitted the complete simulations described in the previous section. The simulation domain was kept small (about  $8 \times 8 \times 8$  wavelengths or  $2.4 \times 2.4 \times 2.4$  km) to permit rapid simulations. Figure 4 describes the simulation results as a snapshot in time.

TN denotes the simulations at step an arbitrarily chosen step N. Figure 44 shows T1 to T3, where the time snapshots 1-3 occurs in increasing time. At T1 we see the wave being injected into the simulation domain. A backward propagating field is seen propagating into the PML. The PML absorbs the backward propagating wave so that it does not scatter into the active simulation domain. For T1, the left plot shows the result in the xz cut-plane, whereas the right plot shows results in the yz cut-plane. The target is located in the center of the simulation space as indicated in the figure. The point target is not an ideal point target, but rather defined as a good conductor occupying an FDTD material cell. The field propagating into the simulation is spherical in nature, but

from a source far away (100km), so that it does not look spherical. Figure 44 shows a view of the injected field, showing its spherical nature.

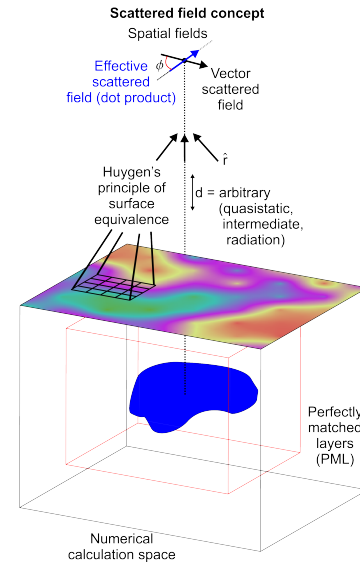


Figure 10. The near-field to far field transform.

When the injected field passes the point-target, energy is scattered toward in the backward direction, causing a strong spherical wave to propagate backwards in T2. In T3, this wave passes through the NFFT boundary and into the PML. The PML absorbs the wave so that it is not reflected back into the active simulations space. The bottom plots in Figure 44 show the electric field components tangential to the NFFT boundary at T3. These results are used by the NFFT transform to calculate the far fields seen at the sensor.

For the 2D comet simulations, the sensor is located at 20km range from the center of the comet. The space between the sensors location and the edge of computational domain is not simulated in order to reduce computational space, as described before. Instead, an analytical-field-propagator (AFP) is used to mathematically inject the fields of the sensor into the top vertical edge of the computation domain [28]. Due to use of TM-z, we use a z-directed dipole at the sensor location and model the exact fields of the dipole at the top interface of the FDTD computational domain. The calculated fields are determined in the frequency domain using the Hankel function in the frequency domain [25], and then converted into the time-domain prior to injection. The E and H fields are injected in a leap-frog manner corresponding to the FDTD method of time-stepping [28]. After this, the simulations are time-stepped until all scattered waves are undetectable. Based on the stability criterion and frequency, this typically corresponds to 3-8k time-steps with a simulation time of about 30-50 minutes on a quad-core Intel 2.8Ghz computer. The RAM memory usage was typically less than about 1 GB. Finally, the scattered fields detected at the top vertical edge were integrated using the modified near-

field to far-field transformation (NFFT) to determine numerically the fields sensed at the sensor dipole [15]. The setup is shown in Fig. 46.

To simulate the circular orbit movement of the sensor, we instead rotated the comet in a counter-direction to that of the intended sensor circular orbit. This is simpler in the sense that only the comet can easily be rotated and re-meshed. For the simulation setup and frequency used here, we used rotation angle step of about 0.3 deg., resulting in about 120 simulations for 0-360 deg. simulations of the comet. This was achieved through parallelization of 6-8 simulations simultaneously within each batch on a multi-core Intel platform. The total duration 0-360 deg. simulations were approximately 2 days. These produced complete radar-grams for the comet imaging radar, which are used with time-domain back-projection to obtain inverted maps of the comet. The radar-grams obtained from the 0-360 simulations contain scattered field solutions from the outer and interior of the comets in time-domain. Often the solutions also include multi-path and multiple reflections and can be ambiguous.

To obtain a spatial dielectric map of the comet, the time-domain back-projection algorithm is used [15]. First, the radar-grams are interpolated using a sinc interpolator and converted into complex values by taking matched filter or convolution with the transmitted analytical signal used in the AFP. The purpose of the complex valued radargram is to obtain a coherent radar signal with accurate phase information of the scattered field. Once the complex valued radargram is obtained, the time-domain back-projection can be initiated. The method used here is known as the pixel-driven methodology, where each pixel in the image back-plane is solved in a sequential manner. A two-dimensional loop is used to sequentially step through all x-y pixels, where pixel size is chosen to be about 10m, which corresponded to the FDTD simulation space Yee-cell discretization as well. For each pixel, the distance from the pixel to each sensor locations (0-360, or about 1200 sensor locations) is calculated. Once the distance to each sensor is known, the interpolated complex field values corresponding to each pixel are found through a search using the nearest neighbor on the range domain. Using this approach the complex value at the pixel is found for all 1200 sensor locations. The pixel target function is calculated as the sum of all complex values at the pixel. This is repeated for every pixel on the image back-plane to obtain an image target function. Finally, the image target function is normalized to obtain a measure of the relative pixel-target signal strength. This image product can be related to the dielectric map when the conductive losses are low, i.e., for low-loss dielectrics such as in most comets. As an additional higher-order correction, we also implemented a ray-bending solution as shown in Figure 46.

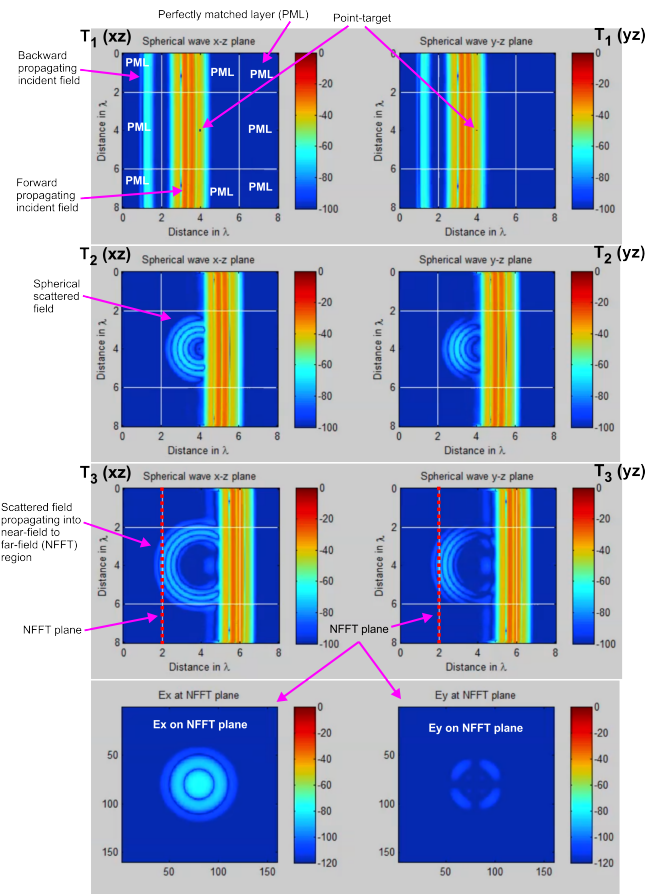


**Figure 11. Three time steps of the point target scattering in 3D. The electric fields on the NFFT plane is a shown for T3**

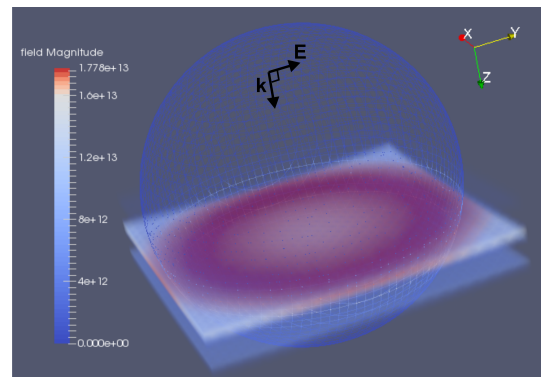


**Figure 12. The spherically injected pulse used in the simulations.**

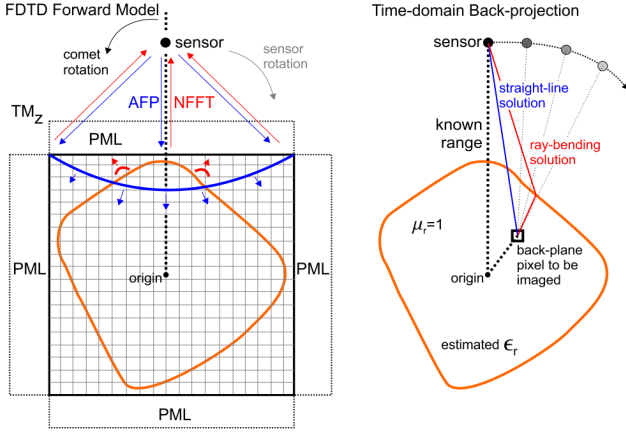


**Figure 13. 2D FDTD forward modeling of the comet and time-domain back-projection to obtain inverted dielectric maps**

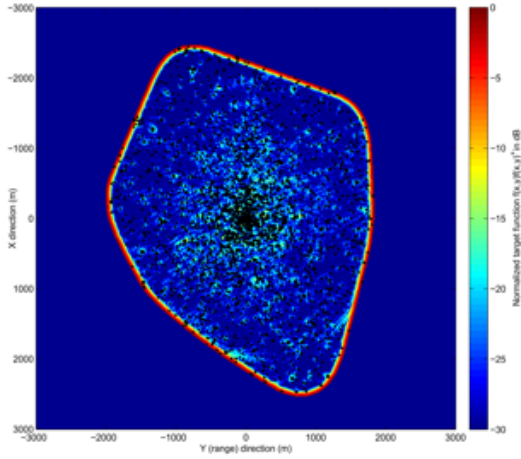


**Figure 14. Time-domain back-projected result of the image for a small inclusion comet model using FDTD.**

Here the propagation is assumed to penetrate the comet at an angle that statistically corresponds to the shortest propagation path between the sensor and the pixel. By assuming knowledge, the comet mean background dielectric, we calculate this shortest path numerically for known comet exterior boundary. This new shortest path is used instead of the direct pixel to sensor range. Figure 47 shows the solution for a model of the comet with 10m resolution and sensor angular step of 0.2 deg. in the circular orbit. The mean relative dielectric permittivity used in about 3.86, which is found from the comet model, and is used in the ray-bending calculations. This model is known as a small-inclusion comet model, where the interior has slowly varying spatial dielectric profile with embedded point-like targets. The point-like targets exhibit some realistic dielectric contrast that can be seen on the back-projected image at values of about -12dB to -20dB. The black dots in the image are the actual targets embedded within the comet. The imaged result shows that the complete AFP-NFFT-FDTD with time-domain back-projection works well to form an accurate image in 2D.

### 5.3. Analytical solutions to scattering using the T-matrix boundary value method

The analytical approaches are developed using series expansions in either the transverse electric and transverse magnetic planes. To simplify the solutions, the theoretical formulations are considered for the two-dimensional case only. With this assumption, the cylinders can be considered semi-infinite along the axis of the cylinder. The cylinders are then used to represent spherical particles in the three-dimensional problem, and thus the solutions are analogous to the extent that the polarization response and the spreading loss differences can be neglected, and particles can be assumed to be located in a 2D space only. The technique can be extended to 3D, however the insight gained from a fully parametrized 3D problem over that of a 2D problem may be inconsequential. The boundary value method uses the solutions of the Hertz potential near the boundary of a collection of semi-infinite cylinders. The cylinders represent particles, and can have an arbitrary size, and dielectric and loss property. A representation of the two-particle system, for simplicity, is shown in Figure 10. The cylinders are non-overlapping, and are located at arbitrary locations in space. The cylinders are located at  $P_i$  and the observation is at location  $P$ . The far-field solution due to plane-wave scattering of a mono-chromatic incoming wave has been given in [12], and the near field solutions of the same problem has been given in [13]. Equivalent circuit techniques can also model the transmissive properties in the microwave band [7]. The medium surrounding the particles can be assumed to be homogenous given by a refracting index  $n$ , and the solutions for electric and magnetic fields can be found by solving the two Hertz potentials [24]:

$$(\Delta + (nk_0)^2) \cdot \begin{bmatrix} u \\ v \end{bmatrix} = 0. \quad (1)$$

Once the solutions to the potentials are known, the fields are given by [24]:

$$\begin{aligned} \vec{E} &= \frac{i}{nk_0} \nabla \times \nabla \times \vec{u} + \nabla \times \vec{v}, \\ \vec{H} &= -n \nabla \times \vec{u} + \frac{i}{k_0} \nabla \times \nabla \times \vec{v}, \\ \vec{u} &= (0, 0, u)^T, \\ \vec{v} &= (0, 0, v)^T. \end{aligned} \quad (2)$$

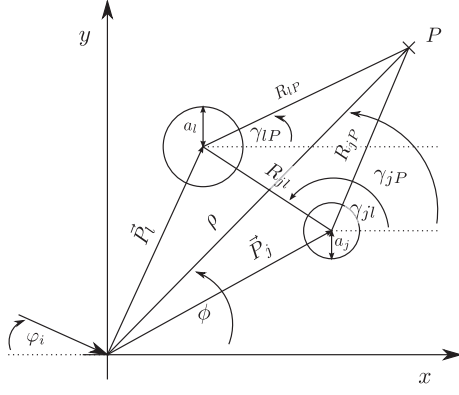


**Figure 15. Description of the multiple particle scattering.**

It is convenient to formulate the problem in the Cylindrical coordinate frame and basis due to the use of semi-infinite cylindrical as 2D representation of particles. In the coordinate frame, as described by Figure 48, the symmetry is chosen along the z-axis, and the z-derivates are therefore non-existent and can be removed from the derivations. Therefore, the solutions to the field equations can be given by:

$$\begin{aligned}
 E_\rho &= \frac{1}{\rho} \frac{\partial v}{\partial \phi}, \\
 H_\rho &= -\frac{n}{\rho} \frac{\partial u}{\partial \phi}, \\
 E_\phi &= -\frac{\partial v}{\partial \rho}, \\
 H_\phi &= n \frac{\partial u}{\partial \rho}, \\
 E_z &= -\frac{i}{nk_0} \left[ \frac{1}{\rho} \frac{\partial}{\partial \rho} \rho \frac{\partial}{\partial \rho} + \frac{1}{\rho^2} \left( \frac{\partial}{\partial \phi} \right)^2 \right] u, \\
 H_z &= -\frac{i}{k_0} \left[ \frac{1}{\rho} \frac{\partial}{\partial \rho} \rho \frac{\partial}{\partial \rho} + \frac{1}{\rho^2} \left( \frac{\partial}{\partial \phi} \right)^2 \right] v.
 \end{aligned} \tag{3}$$

The total potential outside the cylinders can be written as a combination of the incident potentials and due to the scattered potentials [10]:

$$\begin{bmatrix} u^t(P) \\ v^t(P) \end{bmatrix} = \begin{bmatrix} u^0(P) \\ v^0(P) \end{bmatrix} + \begin{bmatrix} u^s(P) \\ v^s(P) \end{bmatrix}, \tag{4}$$

where the superscript 0 denote the incident potentials and the superscript S denote the scattered potentials, whereas the total potentials are given by the superscript t. The incident field potentials are given as [10]:

$$\begin{bmatrix} u^0(P) \\ v^0(P) \end{bmatrix} = \begin{bmatrix} \delta_{TM} \\ 1 - \delta_{TM} \end{bmatrix} \sum_{n=-\infty}^{\infty} (-i)^n e^{in\phi} e^{in\phi_i} J_n(k_m \rho), \tag{5}$$

where the  $J_n$  is a Bessel function of the first kind, and the delta function is used to describe a transverse magnetic or transverse electric solution. The scattered field potentials are given by [10]:

$$\begin{bmatrix} u^s(P) \\ v^s(P) \end{bmatrix} = -\sum_{j=1}^N \sum_{n=-\infty}^{\infty} (-i)^n e^{in\gamma_{jP}} H_n(k_m R_{jP}) \begin{bmatrix} b_{jn} \\ a_{jn} \end{bmatrix}, \tag{6}$$

where the  $H_n$  is a Hankel function of the second kind, and a and b are the expansion constants that can be found by solving a system of equations [24, 10]. For simplicity, we present the co-oriented solutions of the fields, though all components can be found in [24, 10]. For the transverse magnetic solutions, the electric field equation is given by [10]:

$$E_z^s = -ik_m \sum_{j=1}^N \sum_{n=-\infty}^{\infty} (-i)^n e^{in\gamma_{jP}} H_n(k_m R_{jP}) b_{jn}. \tag{7}$$

For the transverse electric solutions, the magnetic field equation is given by [10]:

$$H_z^s = -ik_m n_m \sum_{j=1}^N \sum_{n=-\infty}^{\infty} (-i)^n e^{in\gamma_{jP}} H_n(k_m R_{jP}) a_{jn}. \tag{8}$$

The reader is referred to [24, 10] for the detail derivations and solutions, and for truncation techniques for the summations or series solutions.

#### 5.4 EM Scattering Simulations and Experiments using Granular Media

The problem of using granular media to aid in microwave imaging requires the study of two general bodies of problems. The first general problem involves the vector radiative transfer theory to describe the exact phase sensitive scattering of incident waves by the granular medium, which may be complex in nature with various particle sizes, distributions, and dielectric and conductive properties. The second general problem involves the exact image inversion theory based on phase sensitive scattering of a general distributed scene to be imaged – which may also contain various inclusion/target sizes, distributions, and dielectric

and conductive properties. These two problems can be somewhat decoupled to permit development of each independent of the other. To avoid undue and unnecessary complications, the approach has been to limit the problem to two-dimensions and to use cylindrical media for both the granular medium constituents and the targets in the imaging scene. To permit coherent imaging of the target with aid from the granular media in directing energy, both problems must permit multiple scattering and complex dielectric properties to allow volume currents inside the media, as opposed to just surface scattering found from perfect conducting mediums.

The first problem has been recently addressed using a boundary value method to account for multiple scattering from particles using various sizes, distributions, and complex permittivity values. This approach decomposed the problem into transverse electric (TE) and transverse magnetic (TM) wave components, and solves the boundary conditions for each cylindrical particle using the usual boundary conditions. Presented in a T-matrix solution, the technique permits efficient calculations of the exact plane-wave scattering of TE and TM waves by the arbitrary granular media. See Figure 49.

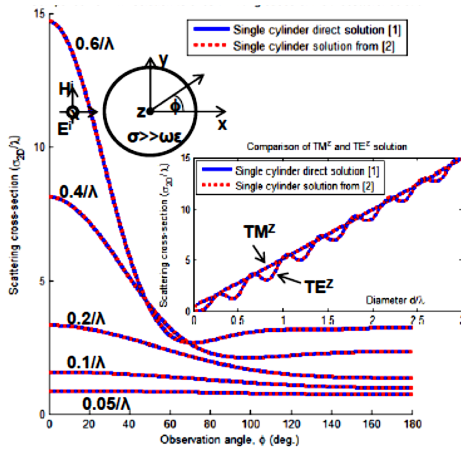


Figure 16. Multiple scattering model applied to a few particles.

The second problem is addressed using a similar technique. The scattered field is computed in a similar manner, but instead of calculating the scattering of the granular media, we calculate the scattering of the target scene. This scattered wave solution is then used to form an image using the time-domain back-projection technique, which projects scattered fields in time into specific pixels within the imaging plane in a coherent manner (Figure 50). To simplify the current development, we use back-scatter from the target scene – therefore describing a mono-static microwave radar problem. The exact scattering permits use of various properties and configurations of the scene to be imaged. We first study the point-target response, where we simulate scattering and then image a collection of small targets, where the targets diameter is significantly smaller than a skin-depth (skin-depth of EM penetration in the target).

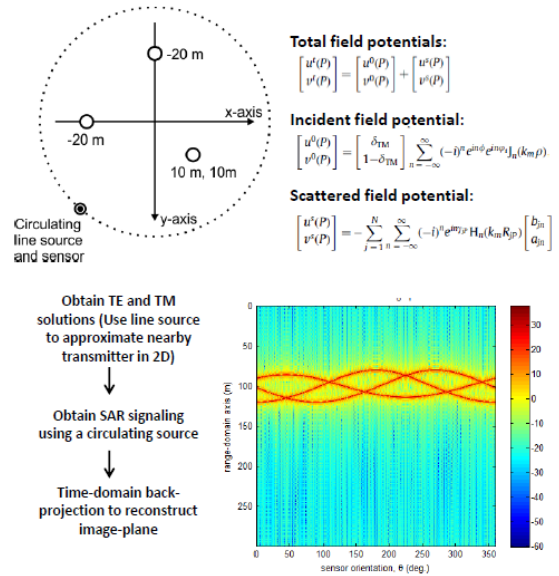
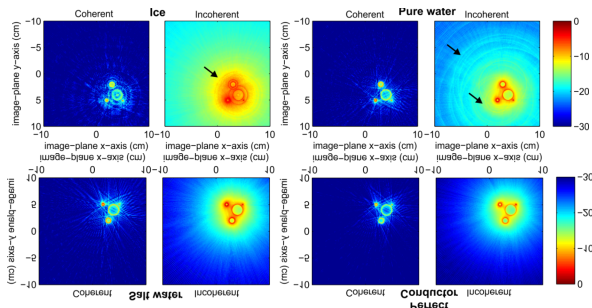


Figure 17. Analytical computation of scattered field.

With the verification of the scattering and imaging complete on point-targets, we next study semi-realistic targets. As an example, the image below shows a small collection of four targets being imaged using coherent and incoherent versions of the time-domain back-projection inversion. The particles are of different sizes and the image-plane is shown for particles that have properties of ice, pure water, salt water, and the ideal target case of perfect conductors (Figure 51). Even in this simple example, we see the artifacts of scattering in the image due to low-loss dielectrics. Coherent imaging is shown to reduce these artifacts considerably when compared to incoherent imaging.

The goal is then to complete the theory and development to study multiple scattering in the imaging plan, and to integrate both granular scattering and imaging problems. The combined analysis will permit a sensitivity analysis of the exact imaging problem in the context of an arbitrary granular medium. The purpose is simple, when a satellite mission is conducting SAR imaging, the imaging resolution is high in the azimuth direction, but low in the cross-track direction. For target bodies with little geophysical activity, this is not problematic since the satellite will eventually sense the whole object and be able to integrate all the data to obtain imaging of the interior. However, for target bodies with high activity, simultaneous cross-track imaging is extremely desirable. While this can be achieved through a second or multiple sensors, there is usually a prohibitive cost associated with additional satellites or sensors.



**Figure 18. Results of tomography analysis for ice and water particles.**

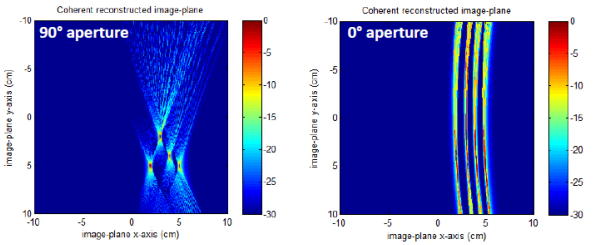


**Figure 19. Sensitivity results for simultaneous cross-track imaging.**

The artifacts due to cross-track imaging is further illustrated using a limited aperture problem and results are shown in Figure 52 to show the benefit of simultaneous cross-track imaging. The images are simulated and back-projected SAR images using an observed aperture in the cross-track. Note that the 90 deg. aperture in cross-track permits a good reconstruction of the 4 targets, whereas with a 0 deg. aperture, extremely poor resolution is obtained (note, the satellite is on the x-axis at  $y = 0$ , thus the arc of solutions for the 0 deg. aperture case).

The above considerations permit us to state that for targets with high geophysical variability in cross-track or inaccessible regions, it is useful to use scattering via some redirected means to image the body. This mechanism of redirection can be achieved via preferential scattering of waves through a granular-based medium. In addition, since higher resolution can be obtained by measuring a wider aperture through use of scattering via a granular media, it is obvious, though observed through Figure 52 as well, that higher resolution can be achieved.

To simulate the effect of the medium, we first obtain a model for the scattering the target body, then redirect scattering through the granular medium. This redirected scattering is essentially a second scattering problem, where the waves scattered from the target body is scattered again by the granular medium. The redirected waves are then focused to the sensor, which collects the energy and focuses the target image in the cross-track. The top left figure below (Figure 53) shows a setup for the simple case of a finite planar cloud mirror. Here the mirror is constructed of a number of closely spaced granular media to form a planar surface that is about  $18\lambda$  wide.

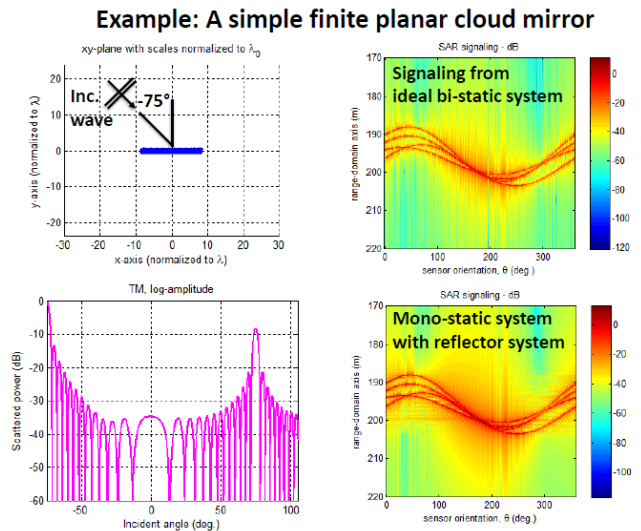


**Figure 20. Scattering result for finite planar cloud mirror.**

Through measurement of the bi-static transverse magnetic  $TM$  scattering, we obtain the angular dependence of the scattered amplitude and phase over the frequencies required for the radar operation. The  $TM$  scattering as a function of scattered angles is obtained for each frequency bin needed for radar imaging. Next, the planar mirror is placed at a desirable location in the problem space such that its reflectance properties become useful to redirect the energy. For example, from the bottom left of Figure 53, it's clear that a substantial reflection cross-section occurs at about  $-75$  deg., so we place this mirror at a location based on that angle. This optimization step is to be discussed in detail in the future.

Once the location is selected, the scattered waves from the target is calculated using the usual scattering theory, and then the scattering function of the granular medium derived previously is used to obtain the scattered field at the sensor. A synthetic aperture in the cross-track is obtained by rotating the medium to image different perspectives of the target body. With the assumption of known scattering function of the granular medium, we can remove the phase perturbation from the granular medium, and are left with the correct amplitude and phase of the redirected signal after removing phase artifacts of the granular medium. This result is shown in the bottom right figure of the same figure. To compare to an ideal representation without the granular medium, we show in Figure 54 the same result using a bi-static measurement on the top right of the same figure. Note that similarities in the result. Note also that the bi-static approach would require a second satellite sensor, whereas the mono-static approach with granular medium only required a single satellite sensor. The result of this, after processing for imaging through SAR approaches is shown below. The figure on the top right is from using a mono-static sensor and granular medium for cross-track SAR imaging.

We studied two critical topics and completed some initial studies on both topics. The first addressed the microwave based imaging or radar imaging of a target, by scattering energy through a granular media. The purpose is to

enable imaging of targets that are either occluded, or to image previously inaccessible parts of the target. This is achieved by re-directing energy through reflection from the granular media. The second topic addresses microwave imaging of the granular media itself, for the purpose of enabling feedback control.

For the first topic, we developed two types of forward simulation methods, one using analytical series expansion of the scattered field – for a quick simulation of scattering from finite spheres (Figure 55), and the second using finite-difference time-domain (FDTD) to simulate full-wave scattering of arbitrarily shaped objects (Figure 56).

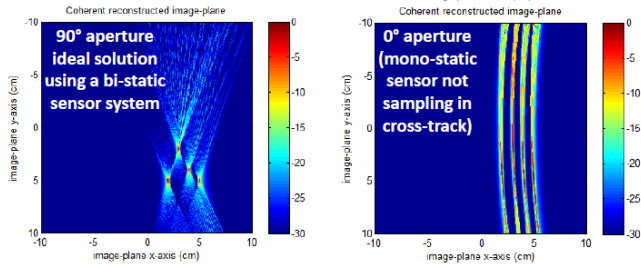


Figure 21. Results for bi-static measurement.

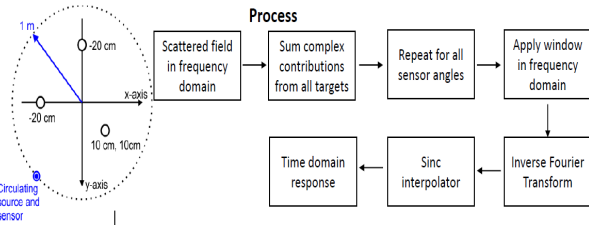


Figure 22. The point-target simulation for quick-analysis of scattering

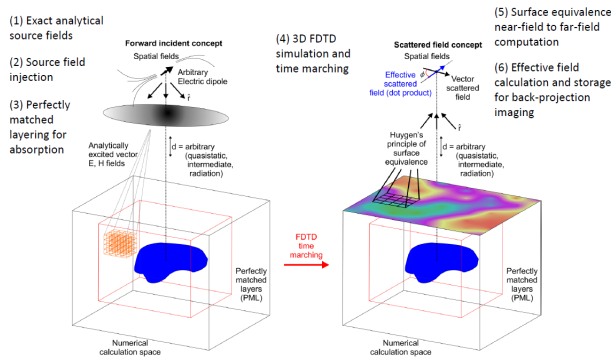
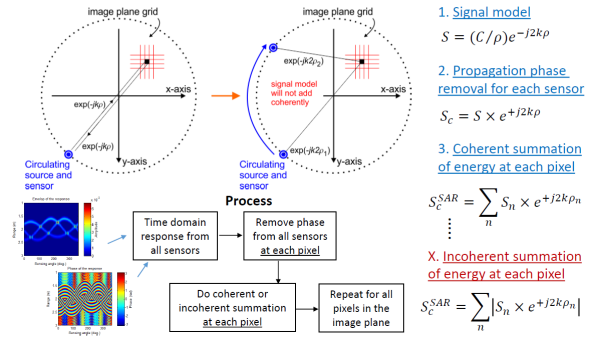


Figure 23. The FDTD technique for full-wave simulation of scattering

We used the simulations to develop a reconstruction algorithm using time-domain back-projection as described in a previous section (Figure 57), and verified that it worked correctly using the simulated results from simple scatterers (Figure 57). In addition, we conducted some simple experiments to first verify the time-domain back-projection algorithm using data collected from a point-target scattering experiment of a small metallic ball collected using a vector

network analyzer (VNA) in free-space and located in an outdoor environment. The ball was held in space and interrogated using a VNA for a wide spectrum of frequencies using a simple wideband horn antenna (see Figure 58).



1. Signal model  
 $S = (C/\rho)e^{-j2k\rho}$
2. Propagation phase removal for each sensor  
 $S_c = S \times e^{+j2k\rho}$
3. Coherent summation of energy at each pixel  
 $S_c^{SAR} = \sum_n S_n \times e^{+j2k\rho_n}$
- ...
- X. Incoherent summation of energy at each pixel  
 $S_c^{SAR} = \sum_n |S_n \times e^{+j2k\rho_n}|$

Figure 24. The time-domain back-projection algorithm.

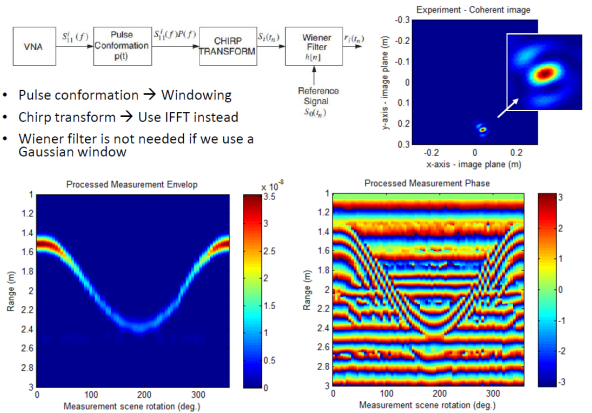


Figure 25. Results from experiments using a VNA and horn antenna over a wide microwave band, and using time-domain back-projection for the inversions.

The next step, was to develop a radiative transfer model that permits multiple scattering from the granular media, in order to re-direct the energy from/to the target. We developed this using exact transverse electric (TE) and transverse magnetic <sup>TM</sup> derivation using electromagnetic potentials and boundary conditions on particles. We used the derivations and approach described in the previous sections to describe the scattering by multiple cylinders using the analytical scattered fields which includes multiple scattering (Figures 59 and 60). Once the transfer model was complete, we studied the re-directing of signaling using some simplified structures for granular media. Specifically, we studied the planar mirror as introduced in Figure 54, with a scheme developed to permit imaging using SAR techniques (Figure 61).

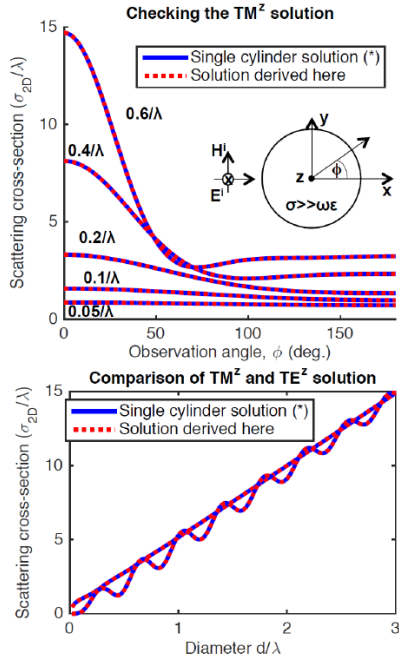
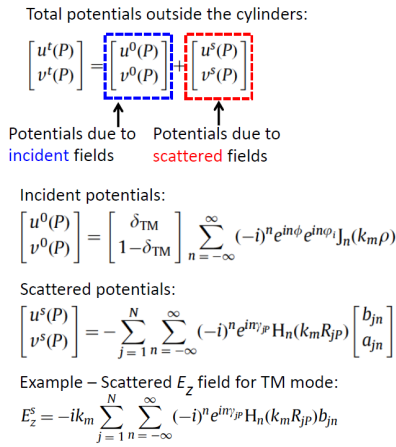


Figure 26. Exact solutions for the radiative transfer from granular media

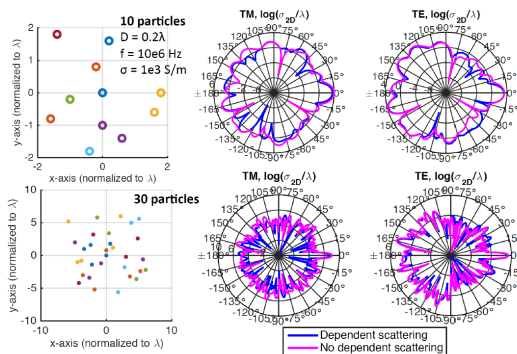


Figure 27. Exact solutions for the radiative transfer from two types of granular media

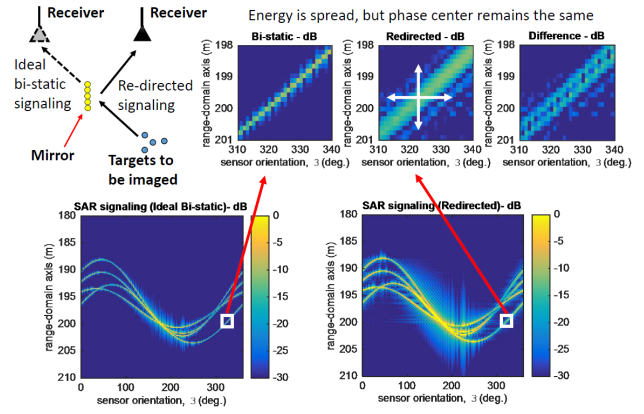


Figure 28. Analysis of re-directed signaling using granular media

The effect of the cloud geometry plays a significant role in the scattering process. In addition, the spatial randomness effects the beam collimation (see Figure 65) and can have an effect on the imaging qualities as it effects effective aperture, coverage, and resolution of the radar techniques. These must be studied to inform about the control of the granular media clouds in space for future re-directed imaging applications.

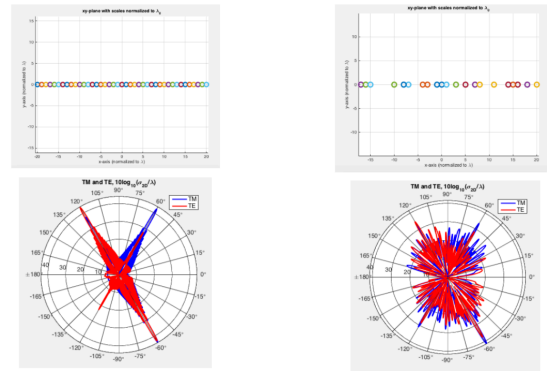


Figure 29. Effect of randomness on system performance as simulated using the analytical field solutions described in the previous sections.

### 5.5. Radar imaging of granular media for feedback control

In addition to the above discussions, we also developed imaging techniques to enable imaging of the granular media for feedback control. We used the cloud physics simulator described in the previous sections, that use point-target scattering functions in cylindrical coordinates, to derive scattered fields from a cloud undergoing variation in time that includes shrinking and rotating cloud configurations. The cloud geometry is described as point-like targets for simplicity, so that the scattered fields are dominated by Rayleigh scattering mechanisms. The exact solutions developed by analytical means are used in two-dimensions to simplify the problem, as implemented in

previous sections. The imaging is achieved in transverse magnetic (TM) basis, again for simplicity, and in addition, the particles are assumed to be good conductors. Figure 66 shows an example of shrinking and rotating cloud configuration chosen to be imaged. The figures show snapshots in time. Figures 67 and 68 shows results for the forward model (exact analytical solutions in TM basis) and inverse solutions using time domain back-projection techniques as described in previous sections. The results show that the general nature and geometry of the cloud can indeed be easily imaged. Higher resolution is expected in the imaging plane by considering wider bandwidths and coherent back-projection algorithms.

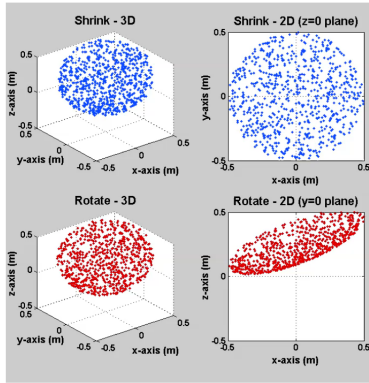


Figure 30. Granular cloud geometry and forward model assumptions.

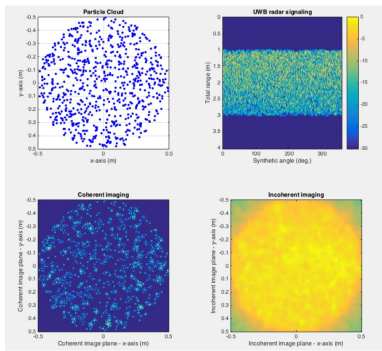


Figure 31. One frame of a video for the imaging of a shrinking cloud.

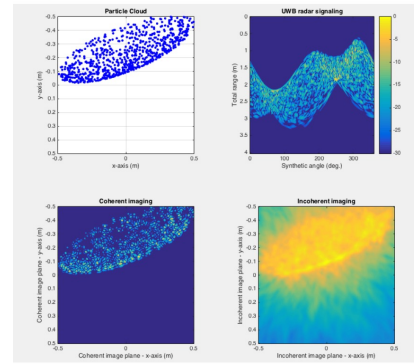
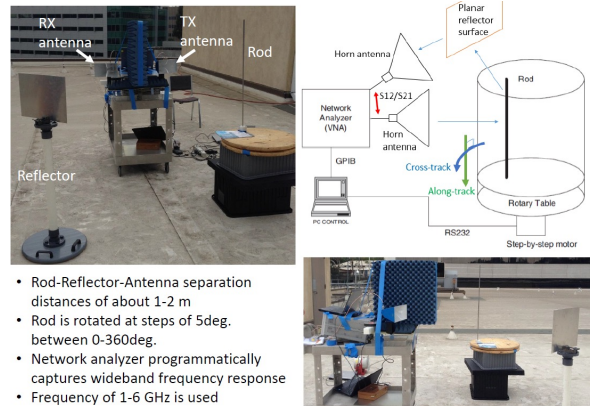


Figure 32. One frame of a video for the imaging of a rotating cloud.

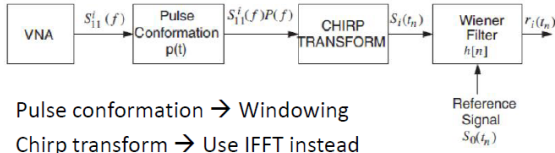
## 6. RADAR EXPERIMENTS

We conducted some experiments to verify the validity of the models and algorithms. In these experiments, we used a planar reflector to re-direct the energy and image a target through the re-directed energy, scattered through the planar reflector. Figure 62 depicts the nature of the experiments conducted. A vector network analyzer is used to measure the scattered electromagnetic fields in the far field of the object to be imaged. For simplicity, the object to be imaged is a simple particle. To further simplify the experiment, we restrict the study to two dimensions, which permit the use of a cylinder to model the particle. We use a rod to model the cylinder or particle in two-dimensions, and use two wide-band horn antennas to generate and sense the fields. A planar finite reflector is used as a simple reflector system to re-direct the energy and fields. A frequency of 1-6 GHz is used.



- Rod-Reflector-Antenna separation distances of about 1-2 m
- Rod is rotated at steps of 5deg. between 0-360deg.
- Network analyzer programmatically captures wideband frequency response
- Frequency of 1-6 GHz is used

Figure 33. Experiments to verify imaging through a planar reflector as an idealized granular media cloud.



- Pulse conformation  $\rightarrow$  Windowing
- Chirp transform  $\rightarrow$  Use IFFT instead
- Wiener filter is not needed if we use a Gaussian window

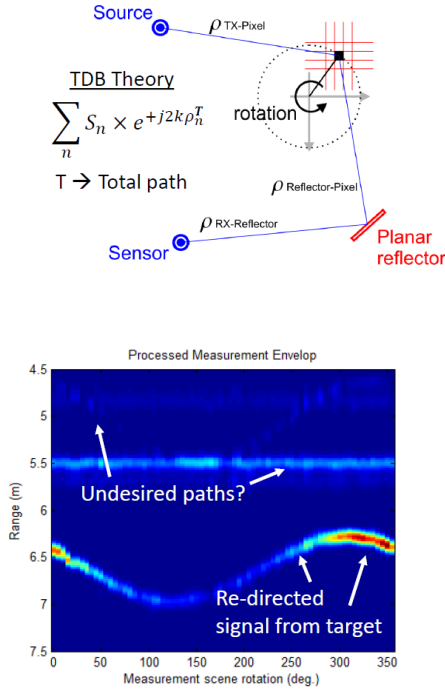


**Figure 34. Results of experiment using a planar reflector as a granular medium.**

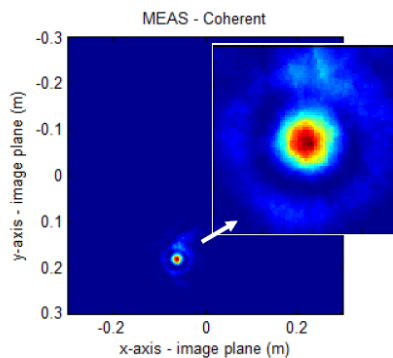


**Figure 35. Inverted results showing target imaging.**

Figures 63 show the results of the experiments and signal processing, along with pulse conformation, chirp transforms, and filtering as well as range gating to remove artifacts of the experiments. The results of the inversions are shown in Figure 64, where the time domain back-projection technique described in a previous section is used. The results confirm the ability to image via a re-directed means using scattered fields through a granular media in space.

## 7. CONCLUSIONS

Inspired by the light scattering and focusing properties of distributed optical assemblies in Nature, such as rainbows and aerosols, and by recent laboratory successes in optical trapping and manipulation, we propose a unique combination of space optics and autonomous robotic system technology, to enable a new vision of space system architecture with applications to ultra-lightweight space optics and, ultimately, in-situ space system fabrication. We call this system the Granular Imager (GI).

The paradigm that makes this granular imager possible is based on: a) avoiding any physical structure and sensing/actuation hardware on the primary aperture, thus lowering the system cost (driven by the mass and complexity of the primary); b) using at-a-distance trapping and manipulation to confine and shape the cloud acting as primary aperture; and c) relaxing the optical figure control requirements by doing the best possible job in software with state-of-the-art computational imaging algorithms.

Typically, the cost of a space-borne imaging system is driven by the size and mass of the primary aperture. The solution that we propose uses a method to construct an imaging system in orbit in which the nonlinear optical properties of a cloud of reflective particles, shaped into a stable surface by electromagnetic means, allow one to form a lightweight aperture of an imaging system, hence reducing overall mass and cost. This new concept is based on recent understandings in the physics of optical manipulation of small particles in the laboratory and the engineering of distributed ensembles of spacecraft swarms to shape an orbiting cloud of micron-sized objects. In the same way that optical tweezers have revolutionized micro- and nano-manipulation of objects, our breakthrough concept will enable new large scale NASA mission applications and develop new technology in the areas of Astrophysical Imaging Systems and Remote Sensing because the cloud can operate as an adaptive optical imaging sensor. While achieving the feasibility of constructing one single aperture out of the cloud is the main topic of this work, it is clear that multiple orbiting aerosol lenses could also combine their power to synthesize a much larger aperture in space to enable challenging goals such as exo-planet detection. Furthermore, this effort could establish feasibility of key issues related to material properties, remote manipulation, and autonomy characteristics of cloud in orbit. There are several types of endeavors (science missions) that could be enabled by this type of approach, i.e. it can enable new astrophysical imaging systems, exo-planet search, large apertures allow for unprecedented high resolution to discern continents and important features of other planets, hyperspectral imaging, adaptive systems, spectroscopy imaging through limb, and stable optical systems from Lagrange-points. Furthermore, future micro-miniaturization might hold promise of a further extension of our dust aperture concept to other more exciting smart dust concepts with other associated capabilities.

Granular media in space can be used in the radar and microwave bands to enable imaging of previously

inaccessible regions of targets with high geophysical variations with time, such as comets. The means of imaging, which includes a re-direction of energy, can permit higher resolution imaging as well. Applications include both tomographic and topographic radar imaging. The effect of the granular media cloud geometry plays a significant role in the scattering process. In addition, the spatial randomness effects the beam collimation and can have an effect on the imaging qualities as it effects effective aperture, coverage, and resolution of the radar techniques. These must be studied to inform about the control of the granular media clouds in space for future re-directed imaging applications. The techniques need to be studied for a specific set of tomographic and topographic applications. The tools and models will need to be advanced to permit application in three-dimensions, which will be required for the application studies. A system engineering study is also needed to study the applicability and feasibility of the technique, as well as an estimate of cost for typical space radar applications where a granular cloud media is to be used. A study is also advised to study the benefits of active vs. passive clouds, which includes imaging, cost, and applications.

#### ACKNOWLEDGEMENTS

© 2017 California Institute of Technology. Government sponsorship acknowledged. This research was carried out at the Jet Propulsion Laboratory, California Institute of Technology, under a contract with the National Aeronautics and Space Administration funded by the NASA Innovative Advanced Concepts (NIAC) program under contract 14-14NIAC-II-0008 (Orbiting Rainbows, Phase II).

#### REFERENCES

- [1] NIAC Phase 1 Final Report on Orbiting Rainbows, [http://www.nasa.gov/directorates/spacetech/niac/2012\\_phase\\_I\\_fellows\\_quadrelli.html#U4KL68bxVEI](http://www.nasa.gov/directorates/spacetech/niac/2012_phase_I_fellows_quadrelli.html#U4KL68bxVEI)
- [2] Quadrelli, M., Basinger, S., Swartzlander, G.: Dynamics and Control of a Disordered System In Space, AIAA SPACE 2013 Conference, San Diego, Ca, Sept. 2013.
- [3] Scott A. Basinger, David M. Palacios, Marco B. Quadrelli, Grover A. Swartzlander: Optics of a granular imaging system (i.e. "orbiting rainbows"), Proceedings SPIE paper 9602-13, SPIE Optics/Photonics Conference, UV/Optical/IR Space Telescopes and Instruments: Innovative Technologies and Concepts VII, San Diego, CA, 9-13 August 2015.
- [4] Quadrelli, B.M., Ius, P., Lanzoni, L.: Modeling and Simulation of Trapping Mechanisms of Granular Media In Space, presented at the AIAA SPACE 2016 Conference, Long Beach, CA, Sept. 2016.
- [5] Marco B. Quadrelli, Scott Basinger, Grover Swartzlander, Darmin Arumugam: Dynamics and Control of Granular Imaging Systems (AIAA 2015-4484), AIAA SPACE 2015 Conference and Exposition, 2015, 10.2514/6.2015-4484.
- [6] Peng, X., Ruane, G., Swartzlander, G., and Quadrelli, B.M.: Randomized Aperture Imaging, Optics Express, 2017.
- [7] Baena J. D., et al., Equivalent-circuit models for split-ring resonators and complementary split-ring resonators coupled to planar transmission lines, in IEEE Transactions on Microwave Theory and Techniques, vol. 53, no. 4, pp. 1451-1461, April 2005.
- [8] Bekey, I.: An extremely large, yet ultra-lightweight space telescope and array, NIAC Phase I report, 1999.
- [9] Bekey, I.: Extremely Large Swarm Array of Picosats from Microwave/RF Earth Sensing, Radiometry and Mapping, NIAC Phase I report, 2005.
- [10] Bohren CF, Huffman DR. Absorption and scattering of light by small particles. New York: Wiley-Interscience; 1998.
- [11] Cubesat NRC report, <http://www.nap.edu/catalog/23503/achieving-science-with-cubesats-thinking-inside-the-box> [NASA2007] Science Plan for NASA's Science Mission Directorate, 2007-2016.
- [12] Xiang Gu; Yunhua Zhang; Xiangkun Zhang, "Near-Field Radar Imaging Simulation using FDTD Method," Antennas, Propagation & EM Theory, 2006. ISAPE '06, 26-29 Oct. 2006. doi: 10.1109/ISAPE.2006.3532
- [13] Lee SC. Dependent scattering of an obliquely incident plane wave by a collection of parallel cylinders. J Appl Phys 1990;68(10):4952-7.
- [14] Lewis, W. E., et al: Geostationary Doppler Radar and tropical cyclone surveillance, J. Atmos. Ocean. Tech., 2011, DOI: 10.1175/JTECH-D-11-00060.1.
- [15] Li, Xu; Taflove, Allen; Backman, Vadim, "Modified FDTD near-to-far-field transformation for improved backscattering calculation of strongly forward-scattering objects," Antennas and Wireless Propagation Letters, IEEE, vol.4, no., pp.35,38, 2005. doi:10.1109/LAWP.2005.845038
- [16] Mettler E., Breckenridge W.G., and Quadrelli M.B.: Large Aperture Telescopes in Formation: Modeling, Metrology, and Control, The Journal of the Astronautical Sciences, vol. 53, no.5 October-December 2005, pp.391-412.
- [17] Mettler, E., et al: Earth atmosphere observatory formation at L2, AIAA Space 2004 Conference and Exposition.
- [18] Michel, R., et al: A Geostationary Optical Seismometer,

Proof of Concept, IEEE Transactions on Geoscience and Remote Sensing, vol. 51, no. 1, Jan. 2012, 695.

- [19] NASA Earth Science Technology Office, "Active and Passive Microwave Technologies Working Group Report", 2004
- [20] NASA ESTO Lidar Investment Strategy Update Community Forum - February 24, 2016
- [21] NASA ESTO Microwave Remote Sensing Investment Strategy Update Community Forum - March 17, 2016
- [22] NRC-DS, 2007: Earth Science and Applications from Space: National Imperatives for the Next Decade and Beyond. National Research Council, The National Academies Press, Washington, D.C., ISBN: 978-0-309-10387-9, 476 pp.
- [23] Peral E., S. Tanelli, Z. Haddad, O. Sy, G. Stephens and E. Im, "Raincube: A proposed constellation of precipitation profiling radars in CubeSat," 2015 IEEE IGARSS, Milan, 2015, pp. 1261-1264. doi: 10.1109/IGARSS.2015.7326003
- [24] Schafer J, Kienle A. Scattering of light by multiple dielectric cylinders: comparison of radiative transfer and Maxwell theory. Opt Lett 2008;33(20):2413-5.
- [25] Understanding the Finite-Difference Time-Domain Method, John B. Schneider, www.eecs.wsu.edu/~schneidj/ufdtd, 2010.
- [26] Smith, E.A., et al: 2007b: NIS White Paper. [Available at <http://nis.ssec.wisc.edu/>]
- [27] A. Taflove and S. Hagness, Computational Electrodynamics - the finite difference time-domain method, 2nd ed. Norwood, MA: Artech House, 2000, pp. 197-201.
- [28] Tan, T.; Potter, M., "Optimized Analytic Field Propagator (O-AFP) for Plane Wave Injection in FDTD Simulations," Antennas and Propagation, IEEE Transactions on, vol.58, no.3, pp.824,831, March 2010. doi: 10.1109/TAP.2009.2039310.
- [29] Yavuz, D.: Frequency and Focal Region Properties of Random Sparse Arrays, IEEE Transactions on Antennas and Propagation, vol. AP-32, no. 5, May 1964.
- [30] Vespoli, J. B., Haber, F., Berkowitz, R., and Yavuz, D., A Self-Organizing Random Array Communication Relay," IEEE Trans. on Communications, No. 4, Apr. 1983, pp.484-492.
- [31] Kerby, K. C. and Bernhard, J. T., Sidelobe Level and Wideband Behavior of Arrays of Random Subarrays," IEEE Trans. on Antennas and Propagation, Vol. 54, No. 8, Aug. 2006, pp. 2253-2262.

## BIOGRAPHY



**Marco Quadrelli** is an internationally renowned expert in modeling for dynamics and control of complex space systems. He has a Masters Degree in Aeronautics and Astronautics from MIT and a PhD in Aerospace Engineering from Georgia Tech. He was a visiting scientist at the Harvard-Smithsonian Center for Astrophysics, and a lecturer at the

Caltech Graduate Aeronautical Laboratories. After joining NASA JPL in 1997 he has contributed to a number of flight projects including the Cassini-- Huygens Probe, Deep Space One, the Mars Aerobot Test Program, the Mars Exploration Rovers, the Space Interferometry Mission, the Autonomous Rendezvous Experiment, and the Mars Science Laboratory, among others. He has been the Attitude Control lead of the Jupiter Icy Moons Orbiter Project, and the Integrated Modeling Task Manager for the Laser Interferometer Space Antenna. He has led or participated in several independent research and development projects in the areas of computational micromechanics, dynamics and control of tethered space systems, formation flying, inflatable apertures, hypersonic entry, precision landing, flexible multibody dynamics, guidance, navigation and control of spacecraft swarms, terramechanics, and precision pointing for optical systems. He is an Associate Fellow of the American Institute of Aeronautics and Astronautics, a NASA Institute of Advanced Concepts Fellow, and a Caltech/Keck Institute for Space Studies Fellow.



**Darmindra Arumugam** is a researcher at JPL/Caltech, specializing in applied electromagnetics. He is the PI and Project Scientist for POINTER, which is an upcoming JPL-DHS mission for first-responder tracking in visually/optically obstructed urban environments.

His current research at JPL also focusses on radar systems and imaging, microwave propagation and scattering theory, and ultra-low-frequency and quasistatic communications and localization. He has pioneered application of localization using quasistatic fields in non-line-of-sight environments, and holds a major patent on this topic. He also actively contributes new algorithms to the MARSIS and SHARAD community, and is an active member of the IEEE, where he routinely publishes in, and reviews for high-impact journals in electromagnetics. Dr. Arumugam is an author in over 40 peer reviewed journals and technical articles. He holds two patents and is routinely invited to review technical articles and proposals in electromagnetics.



